THE INFLUENCE OF RESIN STARVED AREA MANUFACTURING IMPERFECTIONS ON THE MECHANICAL PERFORMANCE OF NON-CRIMP FABRIC CFRP LAMINATE

Susanne Hörrmann[1,2], Adi Adumitroaie[1], Christoph Kralovec[1,2] and Martin Schagerl[1,2]

[1] Institute of Structural Lightweight Design, Johannes Kepler University Linz
Altenberger Straße 69, Aut-4040 Linz, Austria
Email: martin.schagerl@jku.at, web page: http://www.ikl.jku.at

[2] Christian Doppler Laboratory for Structural Strength Control of Lightweight Constructions, Johannes Kepler University Linz
Altenberger Straße 69, Aut-4040 Linz, Austria
Email: susanne.hoerrmann@jku.at, web page: http://www.ikl.jku.at/cd/

Keywords: Non-crimp fabric, Manufacturing Defects, Digital Image Correlation, Experiment, Simulation

ABSTRACT

Resin starved areas or dry spots are considered a severe manufacturing defect in resin transfer molded composite parts, thus often leading to rejects. However, they are rarely mentioned in literature. In this work, the mechanical performance of specimens with artificially introduced resin starved areas under static and fatigue loading is investigated. As a side effect of the defect introduction, the specimen is not symmetrical anymore and some complicated deformation occurs under loading. Displacements, strains and fracture processes are recorded via two 3D DIC systems, on both sides of the specimen. Thereby, the complete sequence of the damage processes during static and fatigue loading can be analyzed. It is found that for this specimen the out of plane displacement is a good indicator for matrix damage and material relaxation. Static failure takes place at the edges surrounding the resin starved area. Fatigue damage is initiated in the resin starved area by longitudinal splitting and fiber fracture, which grows progressively over the whole specimen width.

1 INTRODUCTION

The use of CFRP structural parts in automotive industry is continuously increasing, being triggered mainly by the modern lightweight design concepts, as a means of fuel consumption and carbon emission reduction. In the same time, the automotive industry is continuously seeking for time and cost efficient production methods, in order to remain competitive on a highly dynamic and demanding market. The drawback is that the new efficient production methods for composite parts, such as high pressure resin transfer molding of non-crimp fabrics, show increased amount and types of manufacturing imperfections, which in turn translates in increased variability of the mechanical behavior and parameters throughout the structural parts. Common material imperfections are, for example, fiber waviness, fiber clustering, ply folds and resin rich or resin starved areas.

In previous work it was shown that the occurrence of some imperfections, such as fiber waviness or ply folds, can be considered acceptable depending on their severity and the loading conditions of the part [1, 2]. In contrast, resin starved areas or completely dry spots are considered as the most serious manufacturing defects for composite parts produced through the RTM process [3]. They are usually considered rejects and the production efficiency is accordingly reduced. In general, the production process has to be adjusted to reduce their occurrence. Therefore, the literature on resin starved areas or dry spots usually deals with the parameters influencing the formation of dry spots during processing, such as the resin infusion inlet and outlet points position, geometry and architecture of the dry preforms and preform permeability variations, race tracking at edges of preforms leading to air entrapment, viscosity of the resin, etc. [3-6].

In this work, the mechanical behavior and performance of the composite material featuring resin starved areas are investigated to find acceptance or rejection criteria for parts containing such defects. The material under investigation is a non-crimp unidirectional laminate produced through high pressure RTM, which is used in automotive industry. Resin starved areas and dry spots are induced during impregnation by local compression of the dry preform. Specimens with artificially introduced defects are experimentally analyzed and focus is placed on understanding the damage processes in the defect area in order to provide corrective feedback to manufacturing, and to formulate the quantitative acceptance/rejection criteria for parts affected by such defects.

The complex deformation field at the defect location is evaluated using the 3D digital image correlation (DIC) technique. The experimental results are used to extract qualitative and quantitative information about the damage process and to calibrate the detailed finite element (FE) models of the material with defect, which are in turn used for even better analysis and understanding of the damage initiation and evaluation under different loading situations. Static and fatigue load cases are investigated.

2 EXPERIMENTAL INVESTIGATION

The effect of resin starved areas or dry spots on the static and fatigue strength of UD CFRP is experimentally investigated.

2.1 Material and specimen geometry

Water jet cut CFRP test specimens with artificially introduced resin starved areas are provided by the industry partner. The CFRP material under investigation has a unidirectional (UD) layup $[0]_6$ with a thickness of 2.2 mm and a fiber volume fraction of 45 %. The reinforcement material is an automotive non-crimp fabric (NCF) with an areal weight of 300 g/m². The NCF is warp-knitted with a tricot stitching pattern and polymeric stitching yarn. Glass fibers are used as pillar threads with a spacing of about 2 mm. The matrix constituent is epoxy resin. Specimen plates are manufactured with the high-pressure resin transfer molding process (HP-RTM) in a closed mold.

Resin starved areas are induced into the specimen plates during resin infusion. Square plates with an edge length of 25-30 mm and a thickness of approximately 1 mm are laid onto the dry layup before closing the mold. After consolidation they are removed. Thereby the thickness of the specimen plates is locally reduced to about 1.4 mm while the areal fiber content is constant, which means an increased fiber volume fraction at the defect location. The additional pressure of the inserted plates on the dry preform leads to a locally incomplete wetting of the fibers in the area of the inserted plates. Test specimens are cut out of the CFRP plates such that the resin starved areas are located centrally as indicated in Fig.1. Aluminum tabs are glued onto the specimens to protect them against clamping damage.

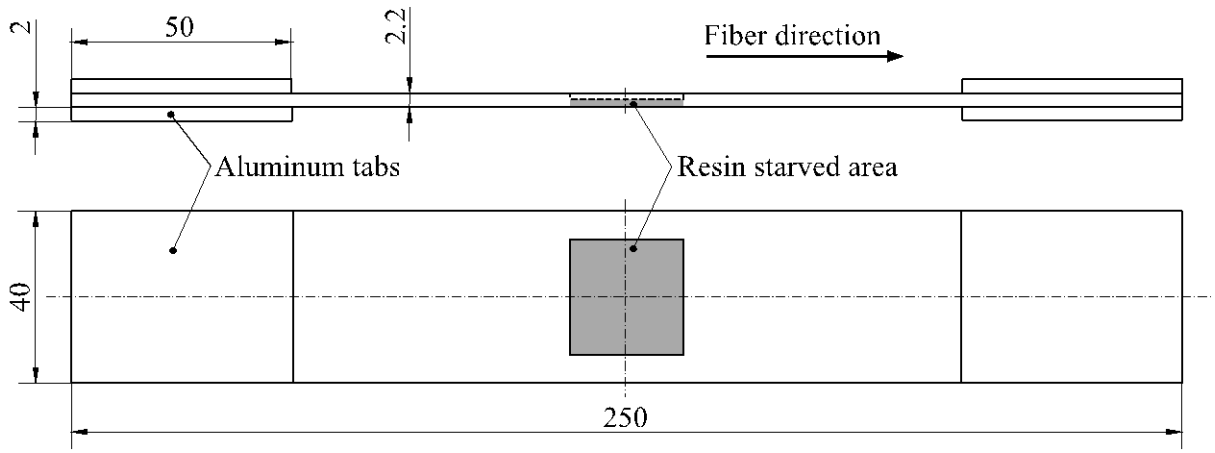

Figure 1: Specimen geometry with resin starved area indicated in gray and including the aluminum tabs (mm as unit of length).

2.2 Non-destructive investigation of the defects

The induced resin starved areas are investigated with non-destructive methods. The local fiber architecture after resin infusion is visualized in the defect area and the expansion of the dry region is determined.

Computed tomography (CT) scans of the defect area are analyzed (Fig. 2(a)). The carbon fiber rovings (light grey) and glass fiber pillar threads (white) can be distinguished. Resin rich regions (darker grey) between the carbon fiber rovings are a result of the polymeric stitching yarn and can mainly be differentiated at the edges next to the resin starved area. Within the resin starved area the fibers are compressed and the fiber volume fraction is much higher (approximately 70 %). This leads to a reduction of the resin rich areas between the rovings. The darker grey spots centrally in the resin starved area do not indicate more resin, but air entrapment or dry fibers. These local spots within the square resin starved area are referred to "dry spots" in the following. It can be observed in the side views, that the dry spots actually occur centrally in the laminate, while on top and bottom the fibers are still impregnated with resin. Shape and size of the dry spots show variability over the investigated specimens.

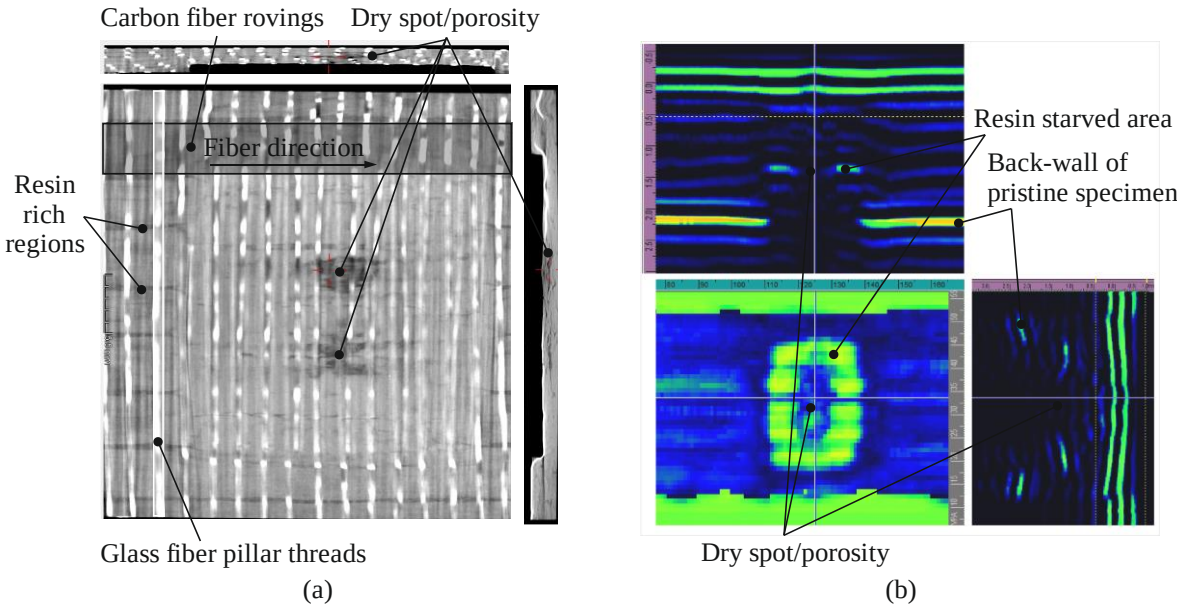

Figure 2: NDT of the resin starved area: (a) CT scan and (b) ultrasonic B- and C-scans.

Ultrasonic scans of all specimens are taken with the pulse echo-method before testing. In Fig. 2(b) the same specimen as in Fig. 2(a) is shown. In the B-scans the back-wall echo of the resin starved area is visible and the thickness reduction can be measured. In the center of the resin starved area no clear back-wall echo exists; this might be because of the diffuse porosity of the dry spot. The size of these areas, where the back-wall echo is lost, is measured for all specimens and is between 80 and 320 mm².

2.3 Test procedure

Static tension tests and constant amplitude tension-tension fatigue tests are performed at ambient temperature. The test rig is equipped with a 100 kN load cylinder and hydraulic wedge grips, which can be used for both static and fatigue loading. An in-house designed alignment device is used to guarantee axial load introduction.

The static tension tests are carried out to investigate the deformation and fracture mechanisms under different tensile load levels. The determination of the tensile strength of the material with defect helps then to define the maximum load levels for the fatigue tests. The static tests are performed displacement controlled with a speed of 2 mm/min. Strain gauges are applied on five specimens and videos of the tests are recorded to capture the damage events. However, because of the inhomogeneous

strain distribution over the specimen surface, full field DIC strain recording is then used instead of strain gauges. The strains of two static tests are measured with two 3D DIC systems (Correlated Solutions and Aramis GOM), one on the front and one on the back side of the specimen.

The constant amplitude fatigue tests are carried out at a frequency of 5 Hz and with a minimum load of 1 kN ($R \approx 0.01$). The maximum loads are iteratively selected between 50 and 70 % of the maximum static tension load, and the reached fatigue life is in the range approximately between 10^3 and $2 \cdot 10^6$ cycles. For the fatigue tests 3D DIC is used to measure the strain field on the backside of the specimen and unlike the static tests 2D DIC is used on the front. Both are triggered on the moments of maximum loading, such that the strain fields of the images can be compared and damage events are recorded.

2.4 Static test results

In total eleven static tensile tests are performed. The maximum load reached is about 64 % of the maximum load of a specimen without defect and the same width and constant thickness. Static tensile loading leads to a series of deformation and fracture events, as described in the following. Some events occur due to the specimen geometry and are not directly triggered by the mere presence of the dry spot.

The measured deformation is mainly due to the asymmetrical specimen geometry as shown in Fig. 1 and 2. This leads to out of plane bending of the resin starved area, in the direction of the front of the specimen from where it was compressed during the resin infusion. The out of plane displacement field for three different load levels of one specimen is shown in Fig. 3; the back side of the specimen is shown on the upper half and the front side is shown on the lower half. Additionally, the average out of plane displacement of the defect area with the applied load is shown in Fig. 4. The solid lines are the front and the dashed lines the back side of the specimens. The displacements are averaged over the squares indicated in Fig. 3.

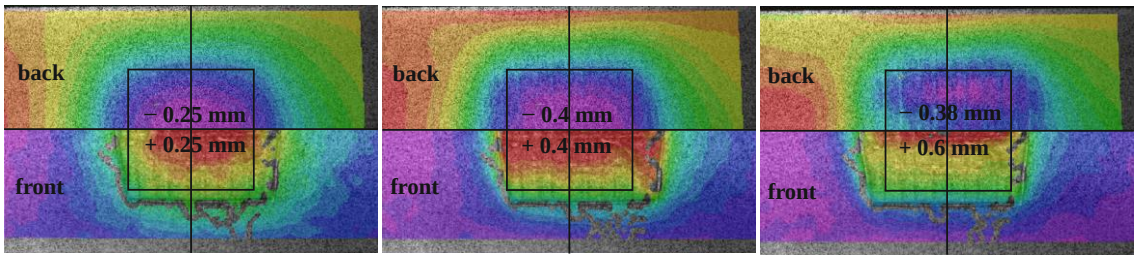

20 % max. F | 60 % max. F | 98 % max. F

Figure 3: DIC measured out of plane displacement field at different static tension loads.

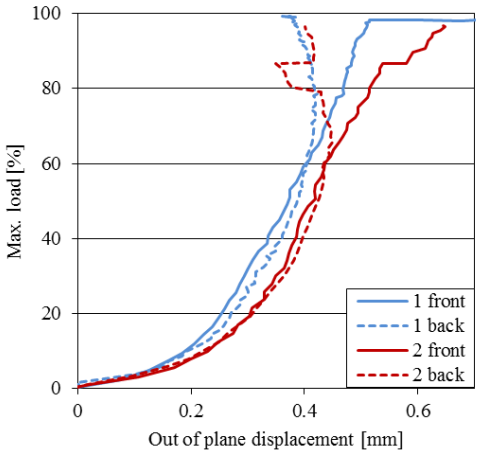

Figure 4: Average out of plane displacement in the resin starved area for two static tests.

The DIC image at 20 % of the maximum load shows, that the dry area is deforming similar to a rectangular plate supported by the surrounding undefected material. Up to 60 % of the maximum load the absolute displacement is identical on back and front of the specimen, and the thickness does not change. At 60 % of the maximum load the deformation gets a rectangular shape, the carbon fibers which were curved during manufacturing due to the local pressing to induce the resin starved area are straight now. Also, the edges of the resin starved area crossing the carbon fibers are bending outwards. When the load is further increased the front and back surfaces start to separate from each other, as it is indicated by the divergent trends of the solid (front side) and dashed (back side) lines in Fig. 4. At 98 % of the maximum load there is a difference of 0.22 mm between the displacements on front and back of the specimen. The thickness of the specimen increases due to matrix cracking and local delamination in the resin starved area and single fiber strands are detached.

For a better resolution and understanding of the defect area deformation out of plane displacements along line cuts through the center of the resin starved area are shown in Fig. 5. Solid lines are the displacements on the front and dashed lines on the back of the specimen. The line cut locations are indicated by black lines in Fig. 3.

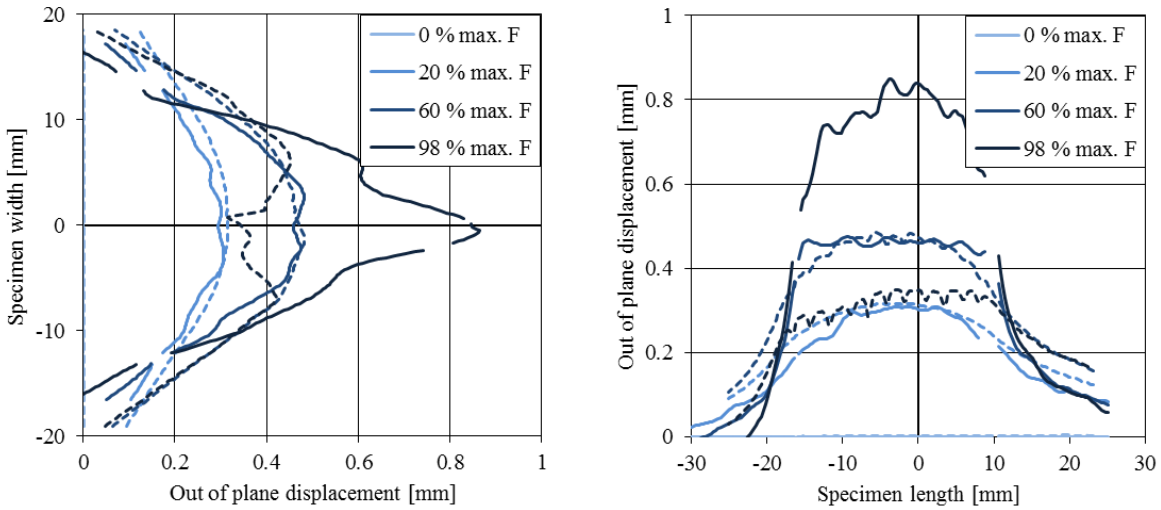

Figure 5: Out of plane displacement distribution along line cuts through the defect area: (a) over the specimen width and (b) over the specimen length.

Up to 60 % of the maximum load the out of plane displacement has a smooth distribution across the length and width of the specimen, and only very small differences exist between the front and back of the specimen. At 60 % the carbon fibers are straightened, and because of this the pattern of the glass fibers becomes visible on the surface of the specimen; this fact is also captured by the 3D DIC reading as slight perturbations in the out of plane displacement field, as it can be noticed in Fig. 5(b), the lines corresponding to 60 % and 98 % loading. For the same reason, the edges of the resin starved area are visible on the front side. At 98 % there is a gap between front and back side displacement lines. Moreover, the pattern of the glass fibers can clearly be seen on the back of the specimen.

Evaluation of the strain distribution shows that the highest difference between the strain in fiber direction on the back and front occurs at about 20 % of the maximum load. With higher loading the strains equalize due to the straightening of the carbon fibers. However, at the same time the glass fibers start to stand out on the surface of the resin starved area and the surface strains are not homogenous any more. The fracture process leading to final failure under static tensile load starts on the backside of the specimen, where there is a region of higher strain in the pristine material near the edges of the defect area, where first fiber fracture occurs. One example is shown in the DIC plots of Fig. 6. Fiber fracture leads to unloading of the broken fibers and thereby to longitudinal splitting as can be seen in the picture at 89 % of the maximum load. With increasing load, more fiber strands progressively fracture leading to final failure.

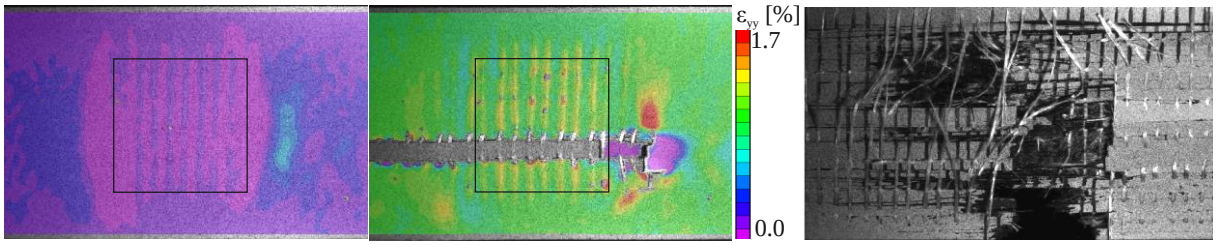

Figure 6: Static fracture process, up to final failure.

Static failure therefore does not initiate inside of the dry spots, but at the edge of the resin starved area due to the specimen geometry, as result from the procedure of defect introduction.

2.5 Fatigue test results

Ten fatigue tests at load levels between 50 and 70 % of the maximum static load are performed. In Fig. 7 the failure points (separation of the specimens) of the fatigue tests are plotted over the number of cycles on a double-logarithmic scale. Three different failure behaviors can be distinguished in Fig. 7, according to the reached number of cycles:

In range ❶ fracture occurs at about 100 cycles. This is usually considered as low cycle fatigue. The fatigue load level is 65 – 70 % of the maximum static load.

In range ❷ fracture occurs between $5 \cdot 10^3$ and $1.5 \cdot 10^4$ cycles at load levels between 54 – 60 % of the maximum load.

In range ❸ the load level is between 50 – 54 %, the specimens did not fail at $2 \cdot 10^6$ cycles and they are considered runouts. This load level gives indication about the endurance limit of the defect material.

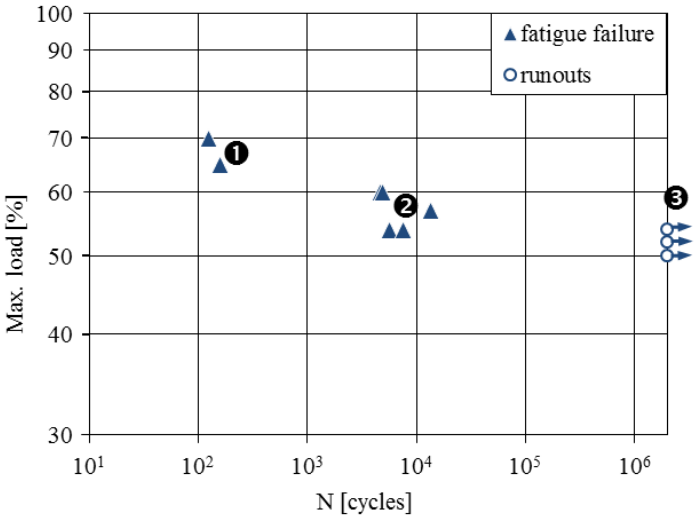

Figure 7: Failure points of the fatigue tests.

The fracture processes at different load ranges are investigated in order to understand how the fracture events are initiated and propagated under fatigue loading; results are compared to the static test results. For this, the out of plane displacement of the backside of the resin starved area is evaluated over the number of cycles.

Specimens which failed in range ❶ show similar fracture behavior as the static tests. First fiber fracture occurs on the backside of the specimens near the edge of the resin starved area (see Fig. 6). Because of this similitude to the static fracture, load range ❶ is not further considered relevant for the fatigue results.

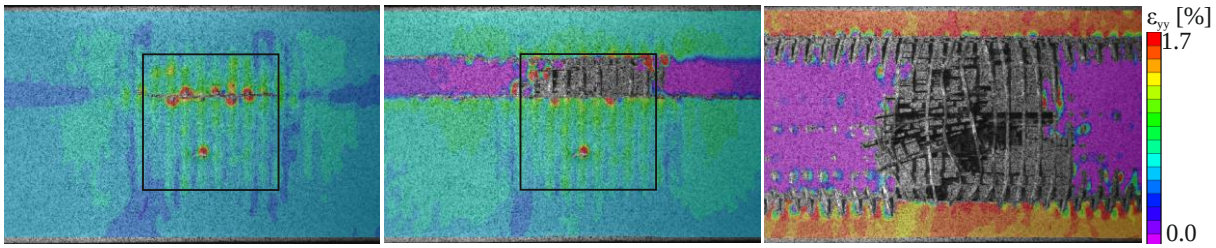

Figure 8: Fatigue fracture up to final failure of the defect material.

The specimens in range ❷ show completely different fracture behavior. One example is shown in Fig. 8: damage is initiated within the resin starved area with longitudinal splitting, which happens at $5 \cdot 10^3$ cycles for the specimen in Fig. 8. Then, individual fiber strands progressively undergo transversal fracture, and thereby they are suddenly unloaded in a spring-back manner; this happens at $5.6 \cdot 10^3$ cycles in Fig. 8. Finally, the fibers of the whole resin starved area are broken and only the sides of the specimen can carry the load for another few cycles. Thus, it is concluded that for the specimens loaded in range ❷ fracture process and final failure occurs in the resin starved area.

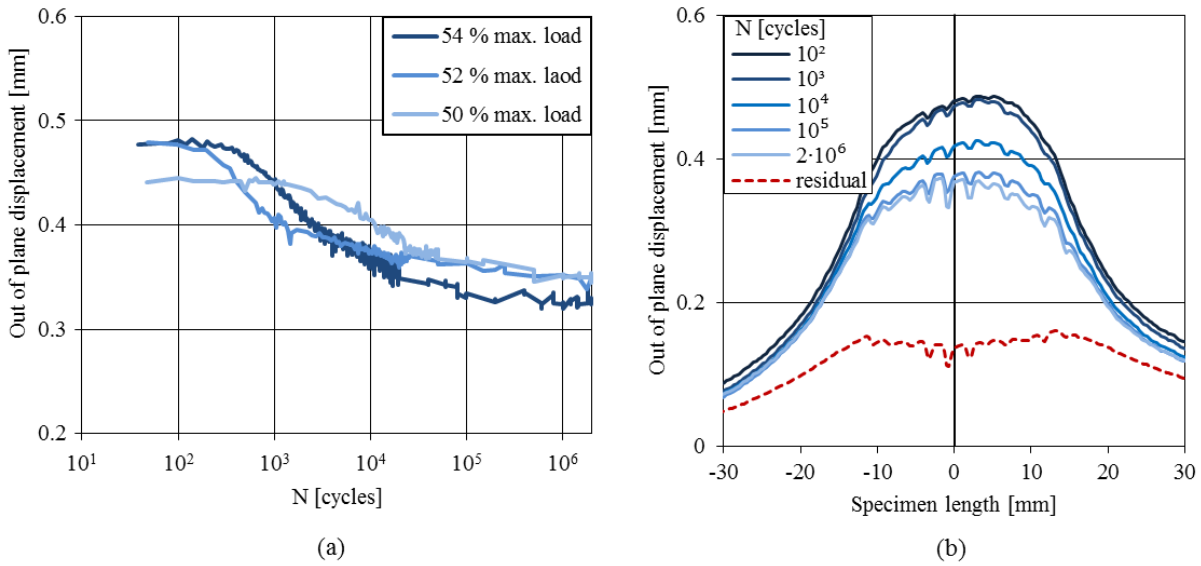

Figure 9: (a) Average out of plane displacement of the runouts and (b) line cuts over the specimen length of the runout with load level of 50 % of the maximum static load.

The runouts ❸ do not finally fail as separate parts, however, relaxation of the resin starved area takes place during the cyclic loading, which indicates progressive fatigue damage inside of the defect area. The out of plane displacements during cyclic loading are recorded with the 3D DIC system and evaluated similar to the static case. The average displacement on the backside of the three runouts over the number of cycles is shown in Fig. 9(a). Over the first few hundred cycles the displacement is constant at its maximum value. Then, it decreases with the number of cycles until it is constant again between $2 \cdot 10^4$ and $2 \cdot 10^6$ cycles. The distribution of out of plane displacement on line cuts over the specimen length is presented in Fig. 9(b) at different numbers of cycles. With increasing number of cycles the pattern of the glass fibers becomes visible. Damage progression represented by out of plane deformation due to cyclic loading is similar to the static test with increasing loading, as shown in Fig. 5(b). However, after reaching $2 \cdot 10^4$ cycles no further damage occurs. The residual deformation after unloading is shown with the dashed line in Fig. 9(b): the specimen is bended inwards, showing a

residual deformation of approximately 0.15 mm. Ultrasonic scans after $2 \cdot 10^6$ cycles also show damages in the resin starved area and in the region of the defect edges.

3 NUMERICAL ANALYSIS

The behavior of the specimens is simulated with ABAQUS 6.14 in a quasi-static geometrically nonlinear analysis. The quarter FE model is built up using quadratic C3D20R elements; the reduced integration element formulation is used in order to avoid the shear locking effects due to the local bending at the defect area. The discretization of the specimen is shown in Fig. 10.

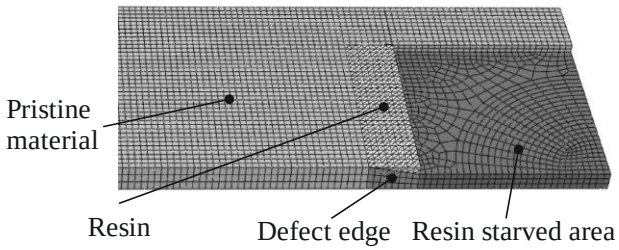

Figure 10: Quarter FE model including sections with different material properties.

Four different sections are defined: the pristine material with orthotropic elastic constants and constant fiber orientation along the specimen length; the resin starved area, where the orthotropic elastic constants are calculated for the higher fiber volume fraction and reduced matrix volume fraction; the volume between the pristine material and the resin starved area (labeled as "defect edge" in Fig. 10), where the fibers are curved towards the resin starved area; the region of pure resin on top of the defect edge with isotropic material behavior. The material properties are given in Table 1. The direction parallel to the fiber direction is indexed by "$\parallel$" and the directions orthogonal are indexed by "$\perp$". The elastic constants for the pristine material are based on previous tests of the same material and on literature. The ones of the resin starved area are calculated using micromechanics formulae to take into account the higher fiber volume fraction and reduced matrix volume fraction. In the defect edge the fiber orientation is aligned with the element edges and the fiber volume fraction is linearly increasing over the number of elements towards the resin starved area, which means that the elastic constants are linearly interpolated between pristine material and resin starved area.

Engineering constant		Pristine material	Resin starved area	Resin
$E_{\parallel\parallel}$	[GPa]	120	176	$E = 4.5$
$E_{\perp\perp}$	[GPa]	10	20	$\nu = 0.3$
$\nu_{\parallel\perp}$	–	0.31	0.31	
$\nu_{\perp\perp}$	–	0.37	0.37	
$G_{\parallel\perp}$	[GPa]	3.4	6.64	
$G_{\perp\perp}$	[GPa]	2.9	5.5	

Table 1: Material properties for the FE model.

Regarding the material properties assigned to the resin starved area in Table 1, it is clear that a more refined method (model) of assessing these values would be desirable. For example, the transverse stiffness in the defect area is not governed only by an increase of fiber volume fraction, and a reduction in matrix volume fraction; it is expected, instead, that the air entrapments over the defect area to give continuous distributions of $E_{\perp\perp}$ over the resin starved area, from a maximum value near the edges of the defect, to zero in the center, where the fibers are completely dry. However, a parametric study over the matrix dominated elastic constants of the resin starved area in Table 1 shows that the effect of these values on the linear elastic deformation is quite low for the given problem. It is

nevertheless expected that a better understanding (most probably based on micro-mechanics modeling of the fibers dry spot inclusion) on how the dry spots contribute to the change of the elastic constants of the resin starved area is necessary when addressing the nonlinear progressive damage behavior of the material in the defect area.

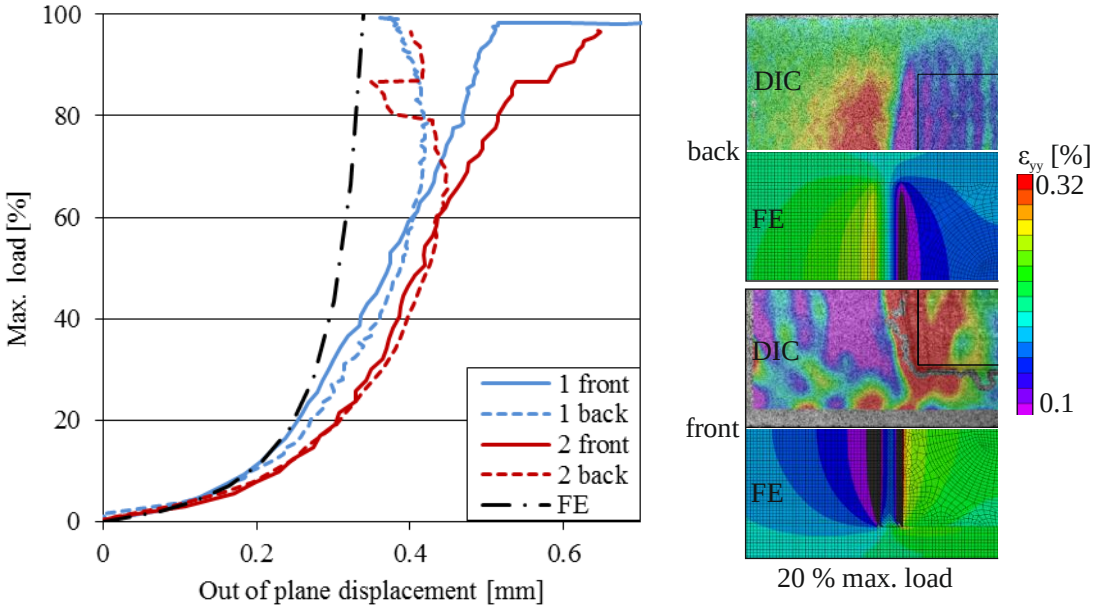

Figure 11: Comparison of FE results and static DIC test results.

In Fig. 11 the results of the FE simulation are compared to the static test results. The average out of plane displacement of the resin starved area is shown on the left diagram. The displacement is similar to specimen 1 up to approximately 20 % of the maximum load. On the right, the strains in load direction at 20 % maximum load are compared. The same color bar is used for the DIC and for the FE results. At this load level the strains match quite well on front and backside. For higher loads the simulated displacement is only marginally increasing. In the real tests matrix cracks and delamination lead to further stiffness degradation of the material, which are not covered by this linear elastic analysis.

4 CONCLUSIONS

The influence of resin starved area manufacturing imperfections on the mechanical performance of a UD non-crimp fabric CFRP material was investigated. For this, resin starved areas with locally dry spots are artificially introduced into specimens which are tested under static and fatigue tensile loading; displacements and strains are monitored with DIC.

Due to the specimen geometry bending is introduced into the resin starved area. It is found that the DIC recorded out of plane displacement of the resin starved area on the front and backside is a good indicator for the damage process which takes place under increasing static tensile loading. Identical damage processes can be observed under fatigue loading with increase of the load cycles, mainly between $5 \cdot 10^3$ and $2 \cdot 10^4$ cycles. Additional cyclic loading does not lead to a damage increase and no final fatigue failure can be observed for specimens, which survive partial damage without failure.

Static failure is initiated by fiber fracture on the backside of the specimen in the pristine material nearby the edge of the resin starved area, where locally regions of high strain are observed. It is concluded that the material of the resin starved area is not the trigger for static failure and therefor the maximum static load should not be used as a general strength value for a resin starved area. Further investigations with different specimen geometry will be necessary to overcome this issue.

Fatigue failure starts with longitudinal splitting along the fibers in the resin starved area and fiber fracture, which progressively spreads over the whole defect area. This fatigue fracture process can be

considered as a direct result of the resin starved material. However, to define the endurance strength of the dry spot the relevant extent of the specimen cross section still has to be defined.

Nonlinear FE analysis of the static test shows good agreement in displacement and strain up to 20 % of the maximum loading. The FE model should be further improved, *e.g.* by inclusion of inter- and intra-laminar progressive damage material non-linearity and more accurate material values of the resin starved area.

ACKNOWLEDGEMENTS

The financial support by the Austrian Federal Ministry of Economy, Family and Youth and the National Foundation for Research, Technology and Development is gratefully acknowledged.

The authors are grateful to Erich Humer for his technical support during the experiments.

REFERENCES

[1] S. Hörrmann, A. Adumitroaie, C. Viechtbauer and M. Schagerl, The effect of fiber waviness on the fatigue life of CFRP materials, *International Journal of Fatigue*, **90**, 2016, pp. 139-147 (doi: 10.1016/j.ijfatigue.2016.04.029).

[2] S. Hörrmann, A. Adumitroaie and M. Schagerl, The effect of ply folds as manufacturing defect on the fatigue life of CFRP materials, *Fracture and Structural Integrity*, **38**, 2016, pp. 76-81 (doi: 10.3221/IGF-ESIS.38.10).

[3] S. Mazumdar, Composites Manufacturing: Materials, Product, and Process Engineering, CRC Press, 2001.

[4] L. Tong, A. P. Mouritz and M. Bannister, *3D Fibre Reinforced Polymer Composites*, Elsevier Science, 2002.

[5] S. G. Advani and E. M. Sozer, *Process Modeling in Composites Manufacturing*, Second Edition, CRC Press, 2010.

[6] E. S. Greenhalgh, *Failure analysis and fractography of polymer composites*, Woodhead Publishing Limited and CRC Press, 2009.